



doi:10.1016/S0016-7037(02)00126-1

## The Geysers-Cobb Mountain Magma System, California (Part 2): Timescales of pluton emplacement and implications for its thermal history

AXEL K. SCHMITT,<sup>1</sup> MARTY GROVE,<sup>1,\*</sup> T. MARK HARRISON,<sup>1,2</sup> OSCAR LOVERA,<sup>1</sup> JEFFREY HULEN,<sup>3</sup> and MARK WALTERS<sup>4</sup>

<sup>1</sup>Department of Earth and Space Sciences, University of California, Los Angeles, 595 Charles Young Dr. E., Los Angeles, CA 90095-1567, USA

<sup>2</sup>Research School of Earth Sciences, The Australian National University, Canberra, A.C.T. 0200, Australia

<sup>3</sup>Energy and Geoscience Institute, University of Utah, 423 Wakara Way, Salt Lake City, UT 84108-1210, USA

<sup>4</sup>Consulting Geologist, 1573 Manzanita Ave., Santa Rosa, CA 95404, USA

(Received July 2, 2002; accepted in revised form February 6, 2003)

**Abstract**—Over 400 ion microprobe U-Pb isotopic ages measured for zircons extracted from 24 geothermal wells that penetrate the Geysers Plutonic complex (GPC) allow us to conclude that the entire known extent of the GPC crystallized during the early Pleistocene. Nine samples of the microgranite porphyry that forms the shallow cupola (100–1,500 m below sea-level, mbsl) of the GPC yield the oldest model U-Pb age ( $1.75 \pm 0.01$  Ma after correction for initial U series disequilibrium; errors  $1\sigma$ ). Twelve samples from the main intrusive phase (orthopyroxene-biotite granite) present at depths  $>1,250$  mbsl define a crystallization age of  $1.27 \pm 0.01$  Ma. This coincides with the age determined for a structurally and compositionally distinct body of granodiorite ( $1.25 \pm 0.01$  Ma;  $N = 5$  samples) that is intruded over a similar depth range. Two petrographically distinct varieties of orthopyroxene-biotite granite yield ages of  $1.46 \pm 0.03$  (GPC21-6000) and  $1.16 \pm 0.02$  Ma (CA5636 74F 21; three samples). U-Pb zircon ages for dikes intruded in metagraywacke country-rocks overlap with those obtained from the main body of the GPC and include the youngest material identified (dike sample NEGU2 ST1-7700:  $1.11 \pm 0.03$  Ma). Overall, the U-Pb results demonstrate that the main body of the GPC ( $\sim 300$  km<sup>3</sup>) was emplaced and crystallized within the upper crust over a short time interval (0.2 Ma) that overlaps with zircon crystallization ages of overlying silicic volcanic units. *Copyright © 2003 Elsevier Ltd*

### 1. INTRODUCTION

The Geysers steam field is the world's largest geothermal reservoir, with a production history dating back to 1955 and a cumulative electrical power capacity of  $\sim 2$  GW (Barker et al., 1992). By virtue of its extensive economic development, it has arguably become the best studied of contemporary modern silicic magmatic-hydrothermal systems (e.g., Kakkonda: Doi et al., 1998; Larderello: Del Moro et al., 1982; Villa and Puxeddu, 1994; Long Valley: Sorey et al., 1978; Taupo Volcanic Zone: Hochstein, 1995; Yellowstone: White et al., 1989). Since its discovery in the early 1980s (Schriener and Suemnicht, 1981), a hypabyssal  $\sim 300$  km<sup>3</sup> (Norton and Hulen, 2001) granite complex, informally known as the “Felsite,” has been demonstrated to provide the dominant structural control for the Geysers steam field. Although it is encountered only in the subsurface, extensive exploration in the form of more than 1000 cumulative km of drill-hole penetrations have revealed that the plutonic body has a northwest trending antiformal shape which coincides with both the early high-temperature hydrothermal aureole and the present-day steam reservoir (Figs. 1, 2; Thompson, 1992; Thompson and Gunderson, 1992; Moore and Gunderson, 1995).

The “Felsite” consists of a complex of petrographically and potentially temporally distinct stocks and dikes (Schriener and Suemnicht, 1981; McLaughlin et al., 1983; Hulen and Walters, 1993; Hulen and Nielson, 1993, 1996; Hulen et al., 1997). Three major units have been recognized (Hulen and Nielson,

1993): shallow microgranite porphyry, orthopyroxene-biotite granite, and an apparently younger hornblende-biotite granodiorite, both at deeper levels (Fig. 2). In recognition of this, Dalrymple et al. (1999) referred to the “Felsite” as the Geysers Plutonic complex or GPC and we adopt the same practice in this paper.

Previous K-Ar, <sup>40</sup>Ar/<sup>39</sup>Ar, and reconnaissance U-Pb zircon geochronologic results have indicated that sampled intrusive rocks of the GPC most likely crystallized more than 1 Ma ago (Dalrymple, 1993; Dalrymple et al., 1999; see Table 1). In spite of this, there has been speculation that portions of the GPC were emplaced much more recently (e.g., Moore and Gunderson, 1995). This belief has been motivated by results of heat flow calculations performed for the Geysers and related areas of high heat flow in the Pliocene-Holocene Clear Lake volcanic field (Fig. 1). These have consistently indicated that a 1 Ma old intrusive bodies of the size of the GPC could not have retained sufficient heat to sustain the modern geothermal reservoir (Donnelly-Nolan et al., 1993; Dalrymple et al., 1999; Norton and Hulen, 2001; Stimac et al., 2001).

Our goal in this paper is to extend the U-Pb zircon work of Dalrymple et al. (1999) by comprehensively sampling the entire GPC and associated dike rocks. A companion study (Schmitt et al., this issue) examines U-Pb zircon and <sup>40</sup>Ar/<sup>39</sup>Ar sanidine age relationships within the volcanic equivalent of the GPC, the Cobb Mountain volcanic center, and assesses conditions of zircon crystallization and crystal residence times for the volcanic system. The results presented here document episodic emplacement and piecemeal assembly of the GPC between  $\sim 1.1$  and  $\sim 1.8$  Ma and firmly indicate that the explored portions of the intrusive complex are too old to have retained

\* Author to whom correspondence should be addressed0 (axel@argon.ess.ucla.edu).

Table 1. Summary of previous age determination of the Geysers Plutonic Complex (GPC).

Well	Depth ft.	Rock <sup>a</sup>	Material	Analysis	Age [Ma]	Error	Reference <sup>b</sup>
CMHC6	8800	felsite	sanidine	<i>K-Ar</i>	1.6	0.4	1
CMHC6	8800	felsite	biotite	<i>K-Ar</i>	2.7	0.3	1
CMHC6	8800	felsite	whole rock	<i>K-Ar</i>	2.5	0.4	1
DV2	6220	microgranite porphyry	feldspar	<i>K-Ar</i>	2.4	0.2	1
FF52 32RD	9100	opx-bt granite	feldspar	<i>K-Ar</i>	1.7	0.2	1
GDC2	7380	opx-bt granite	feldspar	<i>K-Ar</i>	1.9	0.2	1
OF27A	10376	homfels	biotite	<i>Ar-Ar</i>	0.37–1.57	—	2
DV1	(?)	vein	adularia	<i>K-Ar</i>	0.69	0.03	3
PDC2	6630–6830	dike	K-fsp	<i>Ar-Ar</i>	0.57	0.09	4
CA956	(?)	hbl-px-bt granodiorite	feldspar	<i>Ar-Ar</i>	1.1	0.2	4
SB15 D	1548	vein	adularia	<i>Ar-Ar</i>	0.57	0.03*	5
CA958 6	7842	hbl-px-bt granodiorite	K-fsp	<i>Ar-Ar</i>	0.99	0.06	5
CA958 6	7842	hbl-px-bt granodiorite	biotite	<i>Ar-Ar</i>	1.09	0.04*	5
CA 5636 23H 22 <sup>c</sup>	3242	microgranite porphyry	K-fsp	<i>Ar-Ar</i>	1.07	0.03*	5
ANG1	11400	opx-bt granite	K-fsp	<i>Ar-Ar</i>	1.18	0.04*	6
ANG1	11400	opx-bt granite	K-fsp	<i>Ar-Ar</i>	1.05	0.02*	6
ANG1	11440	opx-bt granite	K-fsp	<i>Ar-Ar</i>	1.13	0.08*	6
ANG1	11440	opx-bt granite	K-fsp	<i>Ar-Ar</i>	1.22	0.3*	6
DV2	3708	microgranite porphyry	K-fsp	<i>Ar-Ar</i>	0.67	0.01*	6
FF52	9040	opx-bt granite	K-fsp	<i>Ar-Ar</i>	1.2	0.01*	6
FF52	9040	opx-bt granite	K-fsp	<i>Ar-Ar</i>	1.18	0.01*	6
FF52	9040	opx-bt granite	biotite	<i>Ar-Ar</i>	1.07	0.02*	6
FF52	9140	opx-bt granite	K-fsp	<i>Ar-Ar</i>	1.21	0.07*	6
FF52	9140	opx-bt granite	biotite	<i>Ar-Ar</i>	1.09	0.03*	6
GDC5	7240	opx-bt granite	K-fsp	<i>Ar-Ar</i>	0.91	0.17*	6
GDC5	7240	opx-bt granite	biotite	<i>Ar-Ar</i>	0.93	0.03*	6
GDC5	7800	opx-bt granite	K-fsp	<i>Ar-Ar</i>	0.87	0.02*	6
LF23	9540	opx-bt granite	K-fsp	<i>Ar-Ar</i>	1.14	0.01*	6
LF23	9800	opx-bt granite	K-fsp	<i>Ar-Ar</i>	0.94	0.01*	6
LF23	9800	opx-bt granite	K-fsp	<i>Ar-Ar</i>	0.98	0.02*	6
LF48 <sup>c</sup>	8089	microgranite porphyry	K-fsp	<i>Ar-Ar</i>	0.99	0.01*	6
SB15 D	771–1461	greywacke	illite/smectite	<i>K-Ar</i>	56.27–1.52	—	7

<sup>a</sup> Felsite = undifferentiated.

<sup>b</sup> 1 Schriener and Suemnicht (1981); 2 Unocal (1992) unpublished data.

<sup>c</sup> 3 McLaughlin et al. (1983); 4 Pulka (1991); 5 Hulen et al. (1997); 6 Dalrymple et al. (1999); 7 WoldeGabriel et al. (2001).

<sup>c</sup> Re-classified as opx-bt granite (this study).

\* Terminal age; all others total gas age.

the heat necessary to serve as the primary heat source for the present-day steam field.

## 2. GEOLOGY

### 2.1. Geologic Background

The Geysers geothermal system is centered over a large heat-flow anomaly located in the Coast Ranges of Northern California (Blackwell and Steele, 1992; Fig. 1). The heat-flow anomaly extends northeast from the Geysers where it encompasses Pliocene-Holocene volcanic deposits that define the Clear Lake volcanic field (CLVF in Fig. 1). The CLVF is the youngest and northernmost volcanic center in a series of equivalent features that were formed along the San Andreas Fault since the Miocene (Johnson and O'Neil, 1984). The progressive northwesterly decrease in age of these volcanic fields is well correlated with northward migration of the Mendocino triple junction and concomitant lengthening of the dextral San Andreas transform to form the boundary between the North American and Pacific plates (Dickinson and Snyder, 1979; Johnson and O'Neil, 1984). Formation of a slab window east of the San Andreas fault and the resulting upwelling and decompression melting of mantle rocks and pooling of mantle derived

melts in the continental crust is believed to represent the ultimate driving force for granitic magmatism in the region (see review in Stimac et al., 2001).

The Geysers steam field is situated at the southern edge of the CLVF and partially overlain by 1.2 to 1.0 Ma (Mankinen et al., 1978; Pulka, 1991; Turrin et al., 1994; Schmitt et al., this issue) pyroclastic deposits and lava flows of Cobb Mountain (Hearn et al., 1995; Fig. 1). The GPC and the Cobb Mountain volcanic rocks are aligned between, and are intermediate in age to, the Pine Mountain center in the south and the Tyler Valley center in the north (Fig. 1). The youngest (Holocene) volcanic rocks of the CLVF crop out to the northeast of the Geysers at Mount Konocti (Donnelly-Nolan et al., 1981; Hearn et al., 1995).

The whole area has been interpreted as a pull-apart basin opened between major NW-SE striking faults of the San Andreas transform system (Collayomi, Konocti Bay, Bartlett Springs, Maacama; see Fig. 1) some of which are associated with thermal springs and epithermal gold and mercury deposits (Donnelly-Nolan et al., 1993). Seismic tomography based upon analysis of local earthquakes (Stanley et al., 1998) indicates a northeast trending velocity-high that corresponds in part with the known extent of the GPC. Stanley et al. (1998) related this

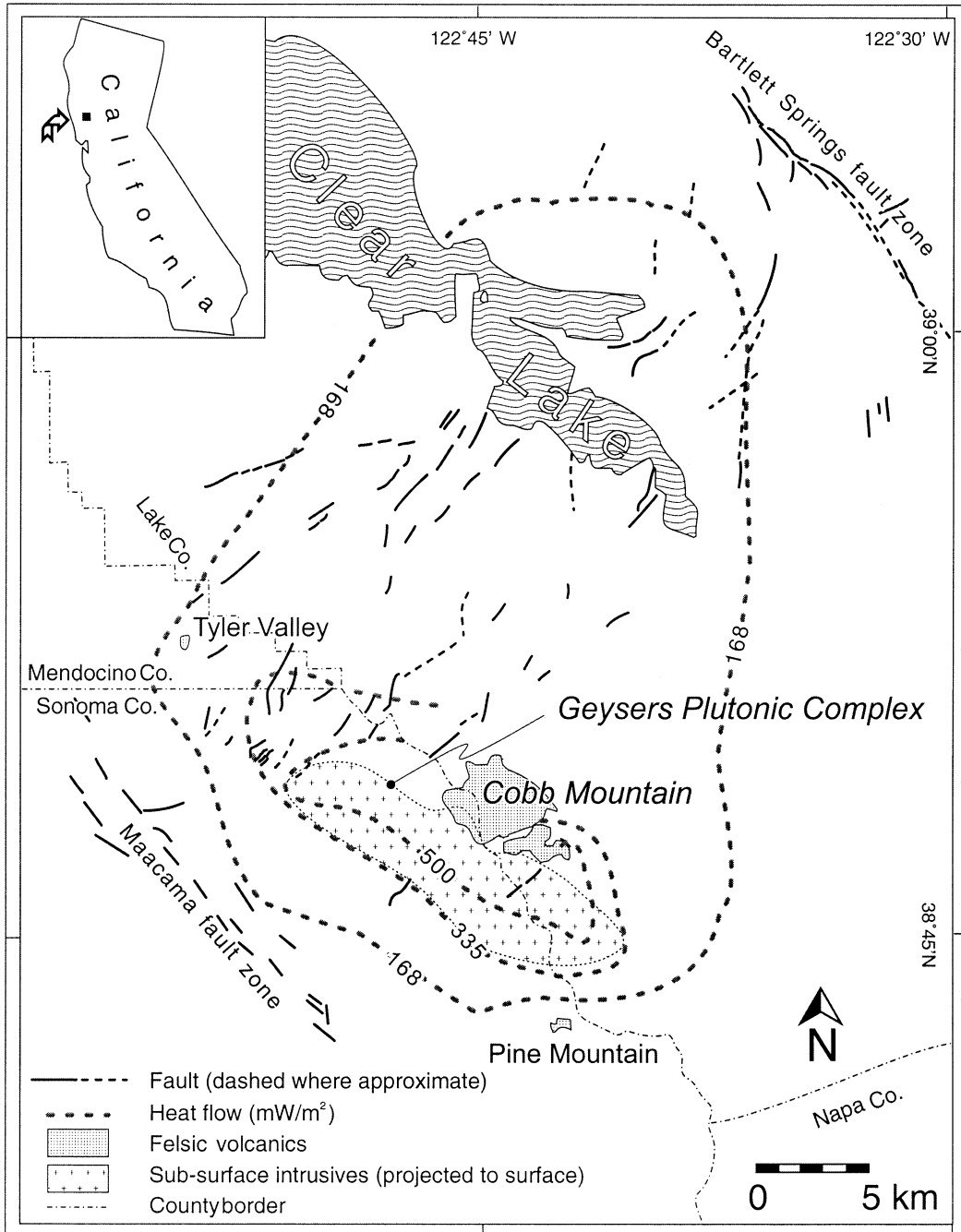


Fig. 1. Heat flow contours and distribution of subsurface plutonic and volcanic rocks of the Geysers – Cobb Mountain system (after Donnelly-Nolan et al., 1981; Walters et al., 1992). Map also shows previously unpublished NE-SW trending tectonic structures in the Clear Lake area. For clarity, only the bounding major NW-SE trending structures of the Bartlett Springs and Maacama fault zones are indicated. For a complete map of tectonic structures, the reader is referred to Donnelly-Nolan et al. (1993) and Hearn et al. (1995).

pattern to concealed intrusions that were emplaced in a north-east trending zone of extension parallel to the direction of maximum horizontal compression (Fig. 1).

**2.2. Geysers Plutonic Complex**

Schriener and Suemnicht (1981) published the first description of an intrusive complex beneath the Geysers steam field.

Since then, both the extent and compositional variations of this wholly concealed plutonic complex and its close relationship to the steam field and the zones of hydrothermal alteration have been well established (e.g., Hulen and Walters, 1993; Hulen and Nielson, 1996; Hulen et al., 1997). The GPC intruded into metagraywackes and related rocks of the Mesozoic Franciscan subduction complex and consists of multiple granite and grano-

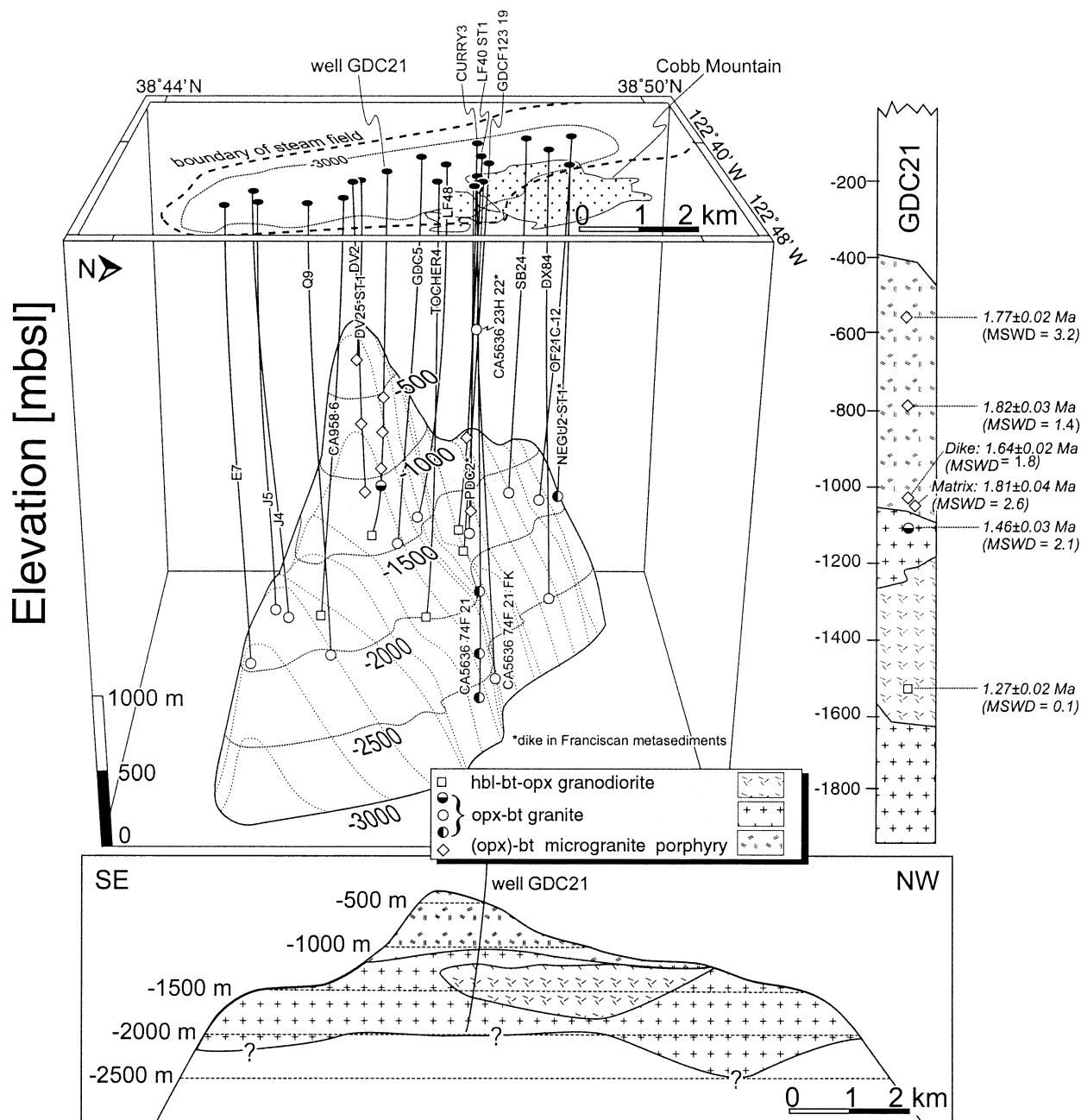


Fig. 2. Three-dimensional structure of the Geysers Plutonic Complex (GPC) after Unocal et al. (1992). Petrologic variations and disequilibrium-corrected average U-Pb zircon model ages are shown for well GDC21 (modified from Hulen and Nielson, 1993) and in a schematized NW-SE cross-section through the central portion of the GPC (distribution and nomenclature for petrologic units from Hulen and Nielson, 1996).

diorite intrusions that compositionally resemble lavas erupted from the overlying Cobb Mountain center (Hulen and Nielson, 1993).

The GPC is first encountered 700 m beneath the surface and broadens downward to a width of 3 km at ~3000 m below sea level (mbsl) (Fig. 2). A 300–600 m wide contact aureole defined by hornfelsed Franciscan metagraywackes was developed around the intrusive complex. Well penetrations have revealed that the both the GPC and enveloping contact aureole

form an elongate, NW-SE trending, 15 km long inverted keel structure (Fig. 2). Its elongate form parallels the trend of NW-SE striking faults that appear to be kinematically related to the dextral San Andreas transform fault system (Fig. 1; Donnelly-Nolan et al., 1981; Donnelly-Nolan et al., 1993).

Previous geochronologic investigations of the GPC primarily employed K-Ar (and  $^{40}\text{Ar}/^{39}\text{Ar}$ ) techniques to in an attempt to either directly date the intrusion of the GPC or indirectly determine the age of hydrothermal alteration and mineraliza-

tion in the overlying reservoir rocks (see summary in Table 1). Most of these efforts were severely hampered by either wall-rock contamination of fine-grained air-drill cuttings (e.g., Schriener and Suemnicht, 1981) and/or by disturbance of the K-Ar system caused by high ambient temperatures, and alteration caused by fluid and gas flow through the reservoir rocks over an extended period of time (see discussion in Dalrymple, 1993). In spite of the interpretative difficulties associated with the Ar isotopic results, they have been used as evidence for very young intrusions within the Geysers field. For example,  $^{40}\text{Ar}/^{39}\text{Ar}$  results as young as 0.6 Ma (Pulka, 1991) led Moore et al. (2000) among others to speculate that intrusions of this age might be present beneath the east central Geysers. Recently, Dalrymple et al. (1999) reported the first U-Pb zircon ages between 1.13 and 1.25 Ma (uncorrected for initial  $^{230}\text{Th}$  deficit) for three samples of the granite phase of the GPC. The present study is an outgrowth of this initial work.

### 2.3. Characteristics of the Hydrothermal System

Two regimes have been recognized within the field for the present-day, vapor-dominated hydrothermal system. In the southeastern and central Geysers, a “normal vapor-dominated reservoir (NVDR)” with preexploitation temperatures of  $\sim 240^\circ\text{C}$  is present. This portion of the field remains in an essentially vaporstatic ( $\sim 3.5\text{ MPa}$ ) condition with no known water table despite drilling to 4 km depth (Moore and Gunderson, 1995). In the northwest third of the Geysers, the NVDR is underlain by a “high-temperature vapor-dominated reservoir (HTVDR)” where temperatures increase with depth from  $240^\circ\text{C}$  to  $340^\circ\text{C}$ . Although this layered system appears to be hosted entirely within Franciscan metagraywacke, the hornfelsed condition of the reservoir rocks suggests that an intrusion underlies the northwestern field (Walters et al., 1992). Chemical trends in the steam and gas compositions clearly differentiate the northwest Geysers from the southeastern part of the field (Lowenstern et al., 1999). In particular the high  $^3\text{He}/^4\text{He}$  ( $R/R_A > 8.3$ ) and low  $^{40}\text{Ar}/^4\text{He}$  ( $< 0.07$ ) ratios in non-condensable gas phase from production wells in the northwest Geysers have been cited as evidence for active magma degassing beneath the northwest Geysers (Kennedy and Truesdell, 1996).

The present-day vapor-dominated reservoir appears to have evolved from a liquid-dominated precursor (Moore and Gunderson, 1995; Moore et al., 2000; Moore et al., 2001). At the early stages, fluid circulation of high-salinity magmatic fluids occurred in the plutonic rocks and the overlying hornfels whereas a second zone of hydrothermal convection that contained preexisting formation water evolved in the overlying metasedimentary cap rocks (Moore and Gunderson, 1995). The transition to vapor-dominated conditions is indicated by the presence of low-salinity fluid inclusions interpreted as condensates from boiling of depressurized hydrothermal liquids at temperatures below  $\sim 300^\circ\text{C}$  (Moore and Gunderson, 1995; Moore et al., 2000).

Numerical simulations indicate that the onset of boiling and fluid venting caused a drop in temperature of the hydrothermal system at the transition from a liquid-dominated to a vapor dominated system (Shook, 1995). Alkali feldspar  $^{40}\text{Ar}/^{39}\text{Ar}$  results have been used to constrain the timing of this rapid-cooling event (Hulen et al., 1997). Integration of hydrothermal

paragenesis and fluid inclusion data with  $^{40}\text{Ar}/^{39}\text{Ar}$  thermal history results performed with vein adularia from the Northwest Geysers (SB15D-1548) indicate that rapid cooling to temperatures  $< 300^\circ\text{C}$  occurred at about 0.26 Ma (Hulen et al., 1997). Similar K-feldspar thermal history results for the central GPC corroborated these results (Dalrymple et al., 1999).

## 3. SAMPLING AND ANALYTICAL METHODS

### 3.1. Sampling

Samples from 24 wells that penetrate the GPC over a broad region were selected for ion microprobe U-Pb zircon age dating (Fig. 2). The selected wells cover the known extent of the GPC and include dike penetrations from outside the main distribution of the GPC. The locations and depth intervals for all samples studied are summarized in Table 2. Note that characters in the sample names left of the hyphenation refer to the well name while those to the right give the depth from the top of the well (in feet, consistent with well-logging practice). With one exception (GDC21-5865), the materials used for zircon separation were fine-grained drill cuttings from geothermal wells. During the drilling process,  $\sim 10$  to  $\sim 100$  g of rock flour were routinely collected at 10 feet ( $\sim 3$  m) depth intervals. In general, we were able to recover sufficient zircon (i.e.,  $\sim 20$  grains) from the material available from a single depth interval. In limited instances, however, it was necessary to combine material sampled from adjacent depth intervals to obtain a sufficient number of zircon crystals.

The cuttings were suspended in heavy-liquids and zircons were hand-picked from the heavy mineral fraction. The only core sample we examined (GDC21-5686) showed cm-scale textural heterogeneity in which a coarse grained dike intruded a fine-grained matrix. We dissected this sample with a diamond wafer saw and crushed the individual parts of the core so that chemical analyses and mineral separates could be obtained separately.

Quantitative X-ray diffraction (XRD) analysis to determine the mineralogical composition of major phases in the samples was performed at the GeoForschungsZentrum Potsdam using a technique specifically designed for analyzing borehole cuttings (Emmermann and Lauterjung, 1990). The detection limit of this approach is between 3 and 5 wt.% and the error in calculated modal abundance is typically between 5 and 10%. Selected samples were also analyzed for major and trace element compositions by standard X-ray fluorescence spectrometry (XRF) at the GeoForschungsZentrum Potsdam (results in Schmitt et al., this issue).

### 3.2. U-Pb Geochronology

U-Pb zircon ages for GPC samples were obtained using the UCLA CAMECA ims 1270 ion microprobe. The companion study (Schmitt et al., this issue) describes sample preparation, instrumental conditions, analytical accuracy and precision of the method. For the age calculations, we first collectively regressed all data from a given sample in a Tera-Wasserburg  $^{207}\text{Pb}/^{206}\text{Pb}$  vs.  $^{238}\text{U}/^{206}\text{Pb}$  diagram in a manner similar to that employed by Baldwin and Ireland (1995). A modified York-regression was used (Mahon, 1996) and concordia was calculated for initial deficit in intermediate daughter isotopes in the U decay chains (in particular  $^{230}\text{Th}$ ). In a second approach, we calculated  $^{206}\text{Pb}/^{238}\text{U}$  ages for individual spot analyses using  $^{207}\text{Pb}$  as an estimator for common Pb (see also Getty and DePaolo, 1995). Both approaches allow for corrections of isotopic disequilibrium caused by fractionation of U and Th during zircon crystallization. Following Schmitt et al. (this issue), we applied a Th/U ratio of 2.3 for the melt and measured Th/U ratio (on average  $\sim 0.36$ ) for zircon. The errors resulting from disequilibrium corrections are small in comparison to calibration and measurement errors. Based on the reproducibility of our standard measurements and a reference zircon with a reported  $\sim 2.5\text{ Ma}$   $^{238}\text{U}/^{206}\text{Pb}$  age (Schmitt et al., this issue), we estimate the overall analytical uncertainties to be  $\pm 3\%$  or less ( $1\sigma$ ). We consistently scaled the analytical errors of the calculated intercept and weighted average ages by the square-root of the MSWD (mean square of weighted deviates) to ensure that they adequately represent experimental scatter and/or sample heterogeneity. We explained this practice in Schmitt et al. (this issue) and

Table 2. Summary of sample locations and Quaternary  $^{238}\text{U}/^{206}\text{Pb}$  zircon ages from GPC. Note that  $1\sigma$  errors have been scaled by the square-root of the MSWD (mean square of weighted deviates) to account for unexplained analytical scatter and/or sample heterogeneity. The numbers of analyzed grains, spot analyses used for calculation of weighted average and excluded analyses (of pre-Quaternary age; see text) is indicated.

Top Bottom Top depth				Remarks	Longitude W	Latitude N	Number		$^{238}\text{U}/^{206}\text{Pb}$ model age [Ma] <sup>a</sup>		$^{238}\text{U}/^{204}\text{Pb}$ model age [Ma] <sup>b</sup>		$^{238}\text{U}/^{206}\text{Pb}$ model age [Ma] <sup>c</sup>		$^{238}\text{U}/^{206}\text{Pb}$ model age [Ma] <sup>d</sup>								
Well	ft.	ft.	m b. sl				spots	grains	excluded <sup>e</sup>	$\pm 1 \sigma$ MSWD	$\pm 1 \sigma$ MSWD	$\pm 1 \sigma$ MSWD	$\pm 1 \sigma$ MSWD										
Microgranite porphyry																							
DV2	3510	3520	-195		-122.7370	38.7680	10	10	1	1.61	0.02	2.3	*	1.60	0.02	1.7	1.75	0.02	2.3	*	1.71	0.02	1.7
DV2	5740	5760	-875		-122.7358	38.7682	10	10	-	1.68	0.07	3.1	*	1.64	0.05	3.1	1.78	0.07	3.1	*	1.77	0.03	3.1
DV25 ST2	5100	5200	-614		-122.7326	38.7692	10	9	-	1.72	0.04	13	*	1.67	0.07	6.0	1.78	0.04	13	*	1.81	0.03	6.0
DV25 ST2	6700	6800	-1102		-122.7309	38.7702	9	9	-	1.83	0.13	8.9	*	1.74	0.11	11	1.92	0.13	8.9	*	1.91	0.04	11
GDCF 123 19	6100	6300	-1049		-122.7849	38.7951	6	6	1	1.65	0.07	9.1	*	1.59	0.23	10	1.74	0.07	9.1	*	1.69	0.07	10
GDC21	4200	4220	-548		-122.7514	38.7746	10	10	-	1.67	0.02	4.0	*	1.63	0.04	3.2	1.76	0.02	4.0	*	1.77	0.02	3.2
GDC21	5000	5020	-792		-122.7507	38.7744	11	11	1	1.74	0.05	3.5	*	1.70	0.04	1.4	1.84	0.05	3.5	*	1.82	0.03	1.4
GDC21	5865	5865	-1056	subsample D	-122.7501	38.7743	10	6	-	1.56	0.05	4.3	*	1.54	0.05	1.8	1.66	0.05	4.3	*	1.63	0.02	1.8
GDC21	5865	5865	-1056	subsample M	-122.7501	38.7742	5	2	-	1.70	0.04	4.9	*	1.68	0.08	2.5	1.80	0.04	4.9	*	1.80	0.04	2.5
PDC2	6720	6750	-1248	dike	-122.7315	38.7937	11	11	-	1.61	0.11	12	*	1.58	0.16	8.4	1.71	0.11	12	*	1.67	0.05	8.4
Orthopyroxene-biotite granite																							
GDC21	6000	6020	-1097	biotite granite	-122.7500	38.7742	10	10	-	1.36	0.01	3.3	*	1.34	0.05	2.1	1.45	0.01	3.3	*	1.46	0.03	2.1
NEGU2 ST1	7700	7840	-1272	dike	-122.7514	38.8155	8	5	-	1.04	0.04	1.5	*	0.87	0.11	1.2	1.13	0.04	1.5	*	1.11	0.03	1.2
CA5636 74F 21	10490	10520	-1966		-122.7479	38.7983	11	11	1	1.15	0.04	3.1	*	1.08	0.11	4.0	1.25	0.04	3.1	*	1.18	0.04	4.0
CA5636 74F 21	11690	11720	-2496		-122.7485	38.7987	15	15	-	1.07	0.03	2.0	*	1.06	0.02	0.97	1.16	0.03	2.0	*	1.16	0.02	0.97
CA5636 74F 21	12890	12920	-2835		-122.7490	38.7992	10	10	1	1.08	0.04	3.8	*	1.03	0.10	5.9	1.18	0.04	3.8	*	1.16	0.07	5.9
DV2	8010	8020	-1563		-122.7332	38.7689	13	13	-	1.28	0.17	9.7	*	1.30	0.18	9.0	1.37	0.17	9.7	*	1.38	0.06	9.0
OF21C 12	9000	9300	-1793		-122.8216	38.8163	12	12	-	1.18	0.06	3.5	*	1.12	0.05	2.1	1.28	0.06	3.5	*	1.23	0.03	2.1
SB24	7600	7940	-1691		-122.8153	38.8082	14	14	-	1.17	0.06	2.5	*	1.19	0.10	5.9	1.26	0.06	2.5	*	1.30	0.03	5.9
CURRY3	8000	8340	-1938		-122.8025	38.7972	14	14	-	1.11	0.05	0.30	*	1.14	0.01	0.05	1.20	0.05	0.3	*	1.25	0.02	0.05
DX84	11300	11340	-2434		-122.7972	38.8179	15	14	-	1.22	0.30	21	*	1.21	0.22	15	1.32	0.30	21	*	1.29	0.05	15
GDC5	8000	8086	-1813		-122.7760	38.7795	14	14	-	1.17	0.05	3.5	*	1.21	0.08	1.9	1.27	0.05	3.5	*	1.26	0.02	1.9
LF48	8020	8080	-1596		-122.7707	38.7840	11	11	-	1.20	0.06	3.1	*	1.13	0.05	2.3	1.30	0.06	3.1	*	1.30	0.03	2.3
CA 5636 74F 21FK	12500	12520	-2713		-122.7535	38.8028	11	10	-	1.15	0.02	0.62	*	1.08	0.03	0.55	1.25	0.02	0.6	*	1.24	0.01	0.55
NCPA J5	9700	10480	-1982		-122.7200	38.7469	17	17	1	1.30	0.09	14	*	1.21	0.18	13	1.40	0.09	14	*	1.33	0.05	13
NCPA J4	8670	9380	-1740		-122.7031	38.7481	17	16	-	1.25	0.04	2.9	*	1.22	0.04	2.5	1.35	0.04	2.9	*	1.33	0.02	2.5
NCPA Q9	9490	9500	-2156		-122.7025	38.7581	14	14	1	1.18	0.01	1.2	*	1.19	0.01	0.23	1.28	0.01	1.2	*	1.26	0.02	0.23
NCPA E7	10070	10100	-2118		-122.6983	38.7414	13	12	-	1.23	0.02	1.4	*	1.16	0.06	1.5	1.32	0.02	1.4	*	1.30	0.03	1.5
CA 5636 23H 22	3242	3262	+24	dike	-122.7347	38.7947	11	7	-	1.22	0.03	0.8	*	1.18	0.21	1.9	1.32	0.03	0.8	*	1.30	0.03	1.9
Hornblende-pyroxene-biotite granodiorite																							
GDCF 123 19	8500	8700	-1781		-122.7859	38.7946	10	10	-	1.23	0.07	5.3	*	1.11	0.06	2.7	1.33	0.07	5.3	*	1.27	0.04	2.7
LF40 ST3	9000	9100	-1793		-122.7641	38.7949	13	13	-	1.14	0.05	1.6	*	1.10	0.02	1.2	1.24	0.05	1.6	*	1.23	0.02	1.2
GDC21	7500	7520	-1554		-122.7492	38.7729	11	11	-	1.15	0.01	0.2	*	1.17	0.01	0.10	1.25	0.01	0.2	*	1.27	0.02	0.10
CA958 6	7842	7862	-1829		-122.7066	38.7611	10	5	1	1.15	0.02	1.9	*	0.72	0.07	0.77	1.22	0.02	1.9	*	1.22	0.04	0.8
TOCHER4	9900	9942	-2068		-122.7356	38.7847	4	4	1	1.15	0.03	0.6	*	1.04	0.10	2.5	1.25	0.03	0.6	*	1.24	0.07	0.2
no Quaternary zircons																							
LF48	6100	6300	-984		-122.7681	38.7850	7	7	-														
CA9586	7290	7300	-1661		-122.7066	38.7611	-	-	-														
TOCHER4	9700	9840	-2007		-122.7356	38.7847	2	2	-														
RA27	9130	9140	-1963	dike	-122.8328	38.8231	1	1	-														
NEGU8	8760	8780	-1860	dike	-122.7640	38.8380	-	-	-														
PRATI25				surface boulder	-122.8418	38.8333	2	2	-														

<sup>a</sup> Y-intercept and concordia intercept age (\* for regression  $R_c^{7/6}$  fixed at 0.8283). <sup>b</sup>  $^{204}\text{Pb}$ -corrected age ( $R_c^{4/6} = 18.8$ ; Sañudo-Wilhelmy and Flegal, 1994). <sup>c</sup> Modified concordia intercept age ( $D_{\text{Th/U}}^{\text{zircon/melt}} = 0.17$ ). <sup>d</sup>  $^{207}\text{Pb}$ - and disequilibrium corrected age ( $D_{\text{Th/U}}^{\text{zircon/melt}}$  from analysis;  $\text{Th}/\text{U}_{\text{melt}} = 2.3$ ). <sup>e</sup> Pre-Quaternary.

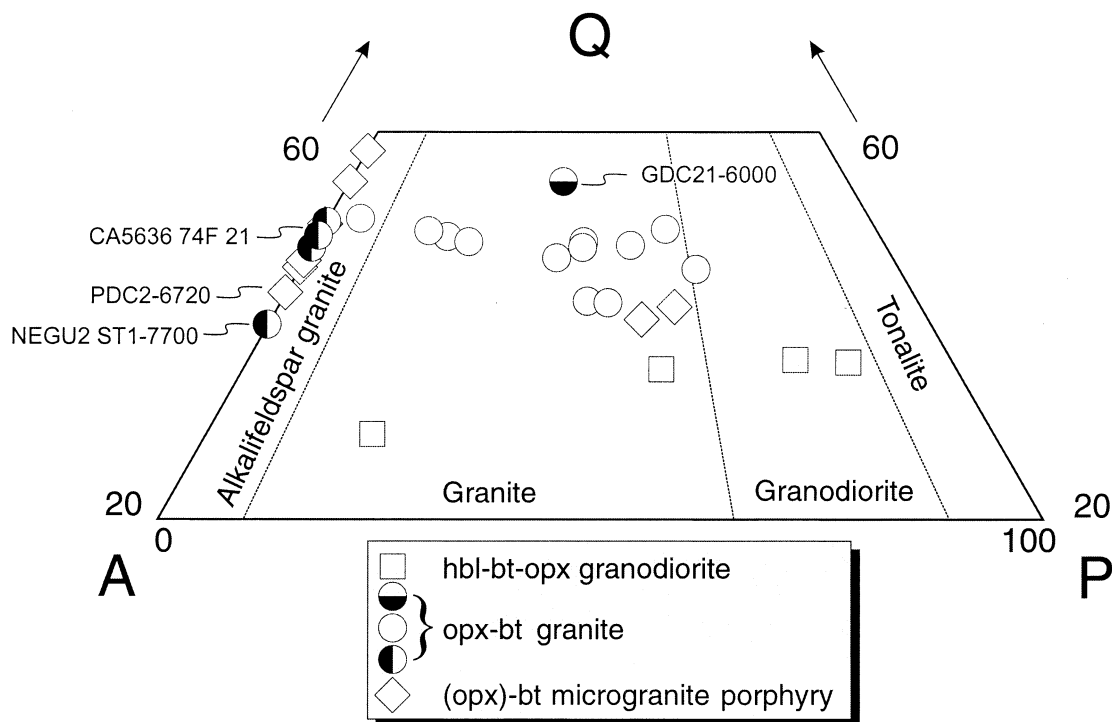


Fig. 3. Classification of GPC drill cutting samples in the QAP (quartz-alkali feldspar-plagioclase) ternary diagram. Nomenclature and compositional boundaries after Le Bas and Streckeisen (1991).

emphasize that this yields a conservative estimate for the age uncertainties in particular for drill-cutting samples that are affected by borehole contamination and small-scale heterogeneities.

## 4. RESULTS

### 4.1. Petrology of the Geysers Plutonic Complex

The original petrologic classification of the GPC rocks was founded on painstaking analysis of fine-grained (<100  $\mu\text{m}$ ) air-drill cuttings, mostly by grain-mount thin section and XRD analysis (Hulen and Walters, 1993; Hulen and Nielson, 1993, 1996; Hulen et al., 1997). Sparse cored materials available from the GPC provided additional textural insights. Hulen and Nielson (1996) interpreted contact relations in hybrid granite (well GDC21) as evidence for magma mixing or partial assimilation of distinct intrusive phases. To ensure that our U-Pb dating study could be placed within this petrologic context, we obtained additional X-ray diffraction (XRD), whole-rock chemical and scanning electron microscopy imaging data. The results of the mineralogical classification are summarized in Figure 2 and Figure 3. A detailed log of one of the deepest wells (GDC21, see Fig. 2; modified from Hulen and Nielson, 1993) and a schematic cross-section further illustrate petrologic variations and internal structures within the GPC. Below we summarize the distribution and the main characteristics of the three main types of intrusive rocks in the GPC based on previous studies (Hulen and Nielson, 1993, 1996) and our additional petrologic analyses.

#### 4.1.1. Microgranite porphyry

Microgranite porphyry forms the uppermost portion of the GPC in the south central Geysers where it is largely confined to the 100–1500 mbsl depth range (see Fig. 2). In the shallowest reaches of this protuberance, the microgranite porphyry is highly altered and silicified. Primary biotite is replaced by chlorite and plagioclase is altered to fine-crystalline white mica. Core materials from well DV2 are intensely brecciated and cemented with secondary quartz-tourmaline vein-fillings. The deeper portion of the microgranite porphyry is comparatively unaltered. In a core sample from this portion (GDC21-5865, Fig. 2) a coarse-grained dike intruded a more fine-grained host, both materials being mineralogically very similar (orthoclase, plagioclase, quartz, pyroxene overgrown by hornblende, and biotite).

#### 4.1.2. Orthopyroxene-biotite granite

Orthopyroxene-biotite granite is encountered throughout the GPC at depths in excess of 1000 mbsl. It dominates the north-western plateau-like portion of the GPC, but also occurs along the more steeply dipping southeast flank (Fig. 2). Quartz contents range from ~40–50% and plagioclase and alkali-feldspar abundances vary widely (Fig. 3). We attribute the latter to hydrothermal alteration and replacement of plagioclase by secondary minerals, in particular sericite. Two petrographically distinct subgroups of orthopyroxene-biotite granite *sensu lato* can be distinguished: in well GDC21 (Fig. 2) a small (~200 m) intercept of “biotite granite” (Hulen and Nielson, 1996) is

present below unaltered microgranite porphyry. It contains more quartz (55 wt.%) and a higher alkali feldspar/plagioclase abundance ratio than unaltered microgranite porphyry. In the eastern part of the field, underlying Cobb Mountain volcanics, well CA5636 74F 21 penetrated exceptionally deep into a previously unstudied portion of the GPC between ~1900 and ~2800 mbsl. This well provided cuttings of a relatively fresh variety of orthopyroxene-biotite granite. In contrast to other samples of the orthopyroxene-biotite granite, the samples in well CA5636 74F 21 are characterized by higher alkali feldspar abundance and abundant relatively unchloritized biotite. Whole-rock major element analysis of CA5636 74F 21 samples yielded SiO<sub>2</sub> contents (normalized to 100% volatile-free) between 76 and 79 wt. %. These values are close to the orthopyroxene-biotite granite from well LF48 (SiO<sub>2</sub> = 76 wt. %; Hulen and Nielson, 1993) but distinctive from the composition of unaltered microgranite porphyry (SiO<sub>2</sub> = 72–73 wt. %; GDC21-5865, Schmitt et al., this issue) and hornblende-pyroxene-biotite granodiorite (SiO<sub>2</sub> = 67 wt. %; CA958 6-7842; Hulen and Nielson, 1996).

#### 4.1.3. Hornblende-pyroxene-biotite granodiorite

Granodiorite is the first intrusive unit encountered in the southeastern GPC at a depth of ~1200 mbsl (Fig. 2). In the central GPC, granodioritic rocks underlie the microgranite porphyry at similar depth levels. When relatively unaltered, granodiorite samples contain abundant plagioclase (~50%), minor alkali feldspar (~15%) and less quartz (~35%) compared to GPC granitic rocks (Fig. 3). Mafic phases are orthopyroxene and clinopyroxene, partially replaced by hornblende, and biotite. The presence of acicular accessory apatite is a characteristic petrographic attribute of the granodiorite (Hulen and Nielson, 1996). The distribution of the granodiorite parallels in shape the NW-SE extension of the orthopyroxene-biotite granite, and in plan view it is either adjacent or enclosed by orthopyroxene-biotite granite. This geometric relationship led Hulen and Nielson (1996) to suggest that the granodiorite intruded the granite.

#### 4.1.4. Dike rocks

Wells at the southeastern margin of the Geysers steam field encountered felsic dikes intruded into hydrothermally overprinted Franciscan metagreywacke beneath Cobb Mountain volcanic rocks. Some of these dikes occur at least 2 km above the main mass of the GPC (Fig. 2). Well logs indicate that they vary in thickness between ~3 and 10 m. Note that a smaller dike thickness would be very difficult to resolve due to the sampling interval and mixing with wall rocks. In this study we selected two dike samples that had been previously targeted for <sup>40</sup>Ar/<sup>39</sup>Ar dating (Pulka, 1991; Hulen et al., 1997) and sampled additional material from wells further to the north (NEGU samples; Fig. 2). All of the dikes have medium- to coarse-grained textures and their modal composition (Fig. 3) classifies them as quartz-rich alkali feldspar granite (PDC2-6720), granite (CA5636 23H 22-3242) and quartz-poor alkali feldspar granite (NEGU2 ST1-7700). Based on mineralogical similarities, we tentatively correlate dike sample PDC2 to the microgranite porphyry phase and CA5636 23H 22 to the orthopy-

roxene biotite granite phase of the GPC main body (Fig. 3). The NEGU2 ST1 sample has low plagioclase content similar to the biotite-rich variety of the orthopyroxene-biotite granite, but contains distinctively less quartz (~40% compared to ~50% in the samples from CA5636 74F 21). Because the amount of dike sample material is small and highly contaminated by fragments of wall rocks, we elected not to perform chemical analyses.

The northwestern region of the Geysers steam field was of particular interest for our sampling, because it is underlain by the distinctive high-temperature, vapor-dominated reservoir (HTVDR, Walters et al., 1992). Unfortunately, no well penetrations of dikes or other intrusives are described for this area. One of us (M.W.) has mapped a house-sized tonalitic block close to the PRATI25 drill-pad, approximately 2 km northwest of the northernmost GPC penetration in well OF21C 12 (Fig. 2). Due to the limited exposure, it was not possible to reliably establish the geologic relations of this block with the surrounding Franciscan tectonomelange. Nevertheless, we included this tonalite for U-Pb dating of zircon and it represents the only surface sample in this study.

## 4.2. U-Pb Zircon Geochronology

### 4.2.1. Wall rock contamination

Petrographic inspection unambiguously revealed evidence for wall-rock contamination in most Geysers air-drill cutting samples we have studied. Fortunately, the much greater antiquity of contaminant zircons contributed by metagreywacke and related lithologies of the Mesozoic Franciscan subduction complex was easily recognized by elevated Pb/U ratios that became evident after only a few minutes of analysis. This obvious contrast allowed us to abort analysis of contaminant zircons and focus our effort upon those derived from the GPC. In most samples the relative proportion of pre-Quaternary grains was <10%. The proportion of contaminant grains increased dramatically in close proximity to the intrusive contacts however. For example, LF48-6100 (positioned just beneath contact with wall-rocks) yielded only one Quaternary age out of seven analyzed grains. In contrast, we measured Quaternary ages in all ten of the zircons analyzed from LF48-8020 in the same well, but situated ~600 m below the contact. In the few cases (n = 24) where we elected to analyze pre-Quaternary grains, we obtained two distinct main groups of concordant U-Pb results (Fig. 4 and Fig. 5): Early Mesozoic (150 - 200 Ma) and medial Cretaceous (90 - 105 Ma). A few pre-Mesozoic zircon grains (300–350 Ma) were also encountered. Zircons with this age distribution are characteristic of the Franciscan subduction complex (Tagami and Dumitru, 1996) and its forearc equivalent (Great Valley sequence – see DeGraaff-Surpless et al., 2002).

### 4.2.2. GPC crystallization ages

Figure 5 shows the distribution of individual <sup>204</sup>Pb-corrected <sup>206</sup>Pb/<sup>238</sup>U ages from the GPC, whereas Table 2 summarizes <sup>206</sup>Pb/<sup>238</sup>U model ages for GPC zircons both before and after correction for initial disequilibrium in the U decay daughter products (data are obtainable from [http://oro.ess.ucla.edu/labdata/data\\_repository.html](http://oro.ess.ucla.edu/labdata/data_repository.html)). All model ages in Table 2 were calculated from at least 3, but typically about 10–15 individual spot

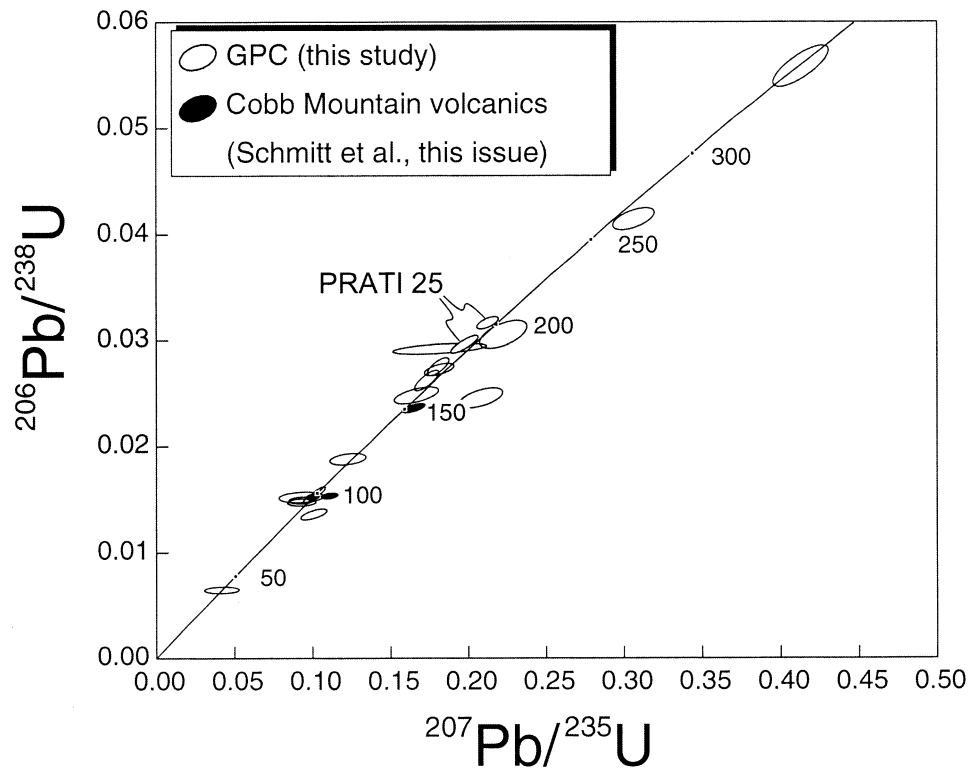


Fig. 4. Results of U-Pb measurements (after  $^{204}\text{Pb}$ -based common-Pb correction) of pre-Quaternary zircons from GPC well samples, surface outcrop of tonalite rock from the northwest Geysers (PRATI25) and Geysers - Cobb Mountain volcanic rocks (Schmitt et al., this issue) plotted with  $1\sigma$  error ellipses (analytical error only).

analyses. Two factors, (1) high U content of GPC zircons; and (2) alternative schemes for applying common Pb corrections have permitted us to obtain the relatively precise results seen in Table 2. Based upon comparisons with reference zircon 91500 (81 ppm U – see Wiedenbeck et al., 1995), zircons from the GPC have U-contents that range between  $\sim 300$  and 19000 ppm with a median of  $\sim 1800$  ppm (Th  $\sim 670$  ppm). The resulting radiogenic  $^{206}\text{Pb}$  yield in the GPC zircons ranges between 10 and 99.5% although this is also strongly dependent on the analytical conditions (see Schmitt et al., this issue). In our companion study on U-Pb zircon dating of volcanic rocks associated with the Geysers, we discussed the high degree of imprecision that resulted when the  $^{204}\text{Pb}$ -correction for common Pb was applied to Quaternary zircons and explored two alternative approaches that allowed more precise  $^{206}\text{Pb}/^{238}\text{U}$  model ages to be calculated: the concordia intercept and  $^{207}\text{Pb}$ -correction method (Schmitt et al., this issue). As indicated in Table 2, both methods yield results that are indistinguishable within error. In contrast we find that use of  $^{204}\text{Pb}$  as a proxy for common Pb produces a systematic ( $\sim 10\%$ ) overcorrection of  $^{206}\text{Pb}/^{238}\text{U}$  ages. We tentatively attribute this overcorrection to the existence of an unresolved interference that contributes to the intensity of the  $^{204}\text{Pb}$  peak.

Two clearly distinct maxima of disequilibrium-corrected  $^{206}\text{Pb}/^{238}\text{U}$  zircon ages (at  $\sim 1.3$  and  $\sim 1.8$  Ma) are evident in Figure 5 (see also Table 2), and the three-dimensional distribution of U-Pb zircon ages is illustrated in Figure 6. Viewing the results as a function of depth (Fig. 6, bottom panel) reveals that the principal source of age variation is lithology. Specifi-

cally, weighted averages of  $^{207}\text{Pb}$ -corrected ages obtained from the shallow microgranite porphyry are distinctively older, ranging between 1.63 and 1.91 Ma (weighted average of  $1.75 \pm 0.01$  Ma; MSWD = 7.1; N = 9 samples; n = 71 grains). In contrast, younger and overlapping ages were obtained for the underlying orthopyroxene-biotite granite (1.23–1.38 Ma; weighted average of  $1.27 \pm 0.01$  Ma, MSWD = 2.4; N = 12; n = 159) and granodiorite (1.22–1.27 Ma; weighted average of  $1.24 \pm 0.01$  Ma, MSWD = 0.69; N = 5; n = 41). Age vs. longitude or latitude relations (Fig. 6) show no systematic variations. For example, ages obtained for the orthopyroxene-biotite granite from the extreme northwest and the southeast GPC are indistinguishable within analytical precision.

By virtue of the availability of cored material from GDC21, this well offers the best constrained intrusive relationships within the GPC. Three samples from the microgranite porphyry in well GDC21 (Fig. 2) were sampled at 549 (GDC21-4000), 792 (GDC21-5000) and 1056 mbsl (GDC21-5686). The results for sample GDC21-4200 and GDC21-5000 overlap within error ( $1.77 \pm 0.02$  Ma; MSWD = 3.2; n = 10 and  $1.82 \pm 0.03$  Ma; MSWD = 1.4; n = 10, respectively), and agree well with the weighted average of five spot analyses on the only two zircons grains that could be obtained from fine-grained microgranite sample GDC21-5686M ( $1.81 \pm 0.04$  Ma; MSWD = 2.6; n = 2). Zircon grains from sample GDC21-5686D, a coarse-grained dike that is in intrusive contact with the fine-grained microgranite, yielded a somewhat younger age of  $1.62 \pm 0.02$  Ma (MSWD = 1.8; n = 6). Interestingly, material from well GDC21 produced another result that is

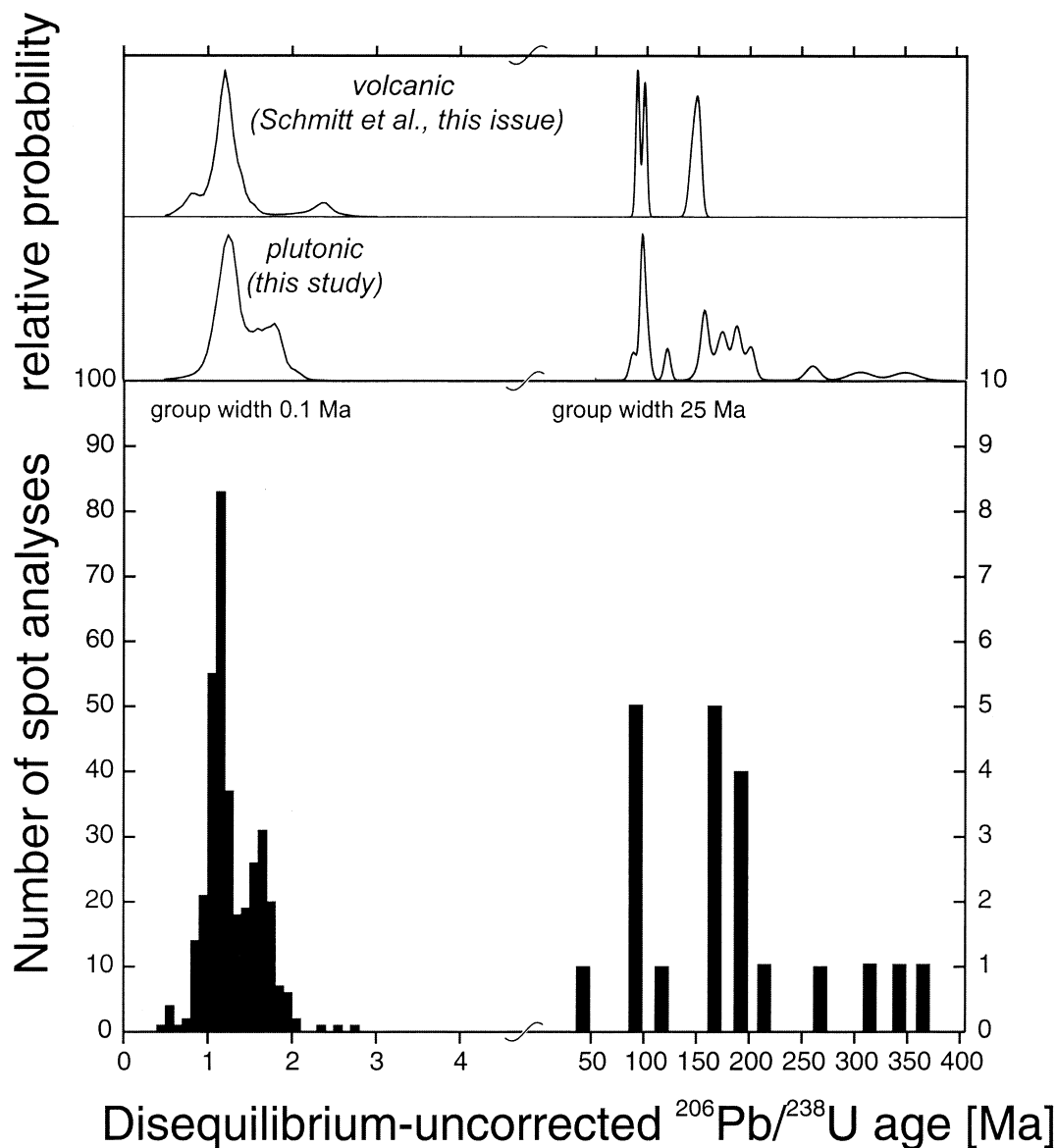


Fig. 5. Histogram showing age distribution calculated from individual  $^{238}\text{U}/^{206}\text{Pb}$  zircon model ages of GPC samples. Ages were calculated after a  $^{207}\text{Pb}$ -based common lead correction, but are uncorrected for initial disequilibrium. Note different scales for Quaternary ( $n = 383$ ) and pre-Quaternary ages ( $n = 26$ ). For comparison between plutonic and volcanic samples, see normalized probability density curves in upper panel. Note the virtual absence of zircons  $<1$  Ma.

intermediate between the U-Pb ages typically obtained from the microgranite porphyry and the granite and granodiorite units. Drilled at levels intermediate between the microgranite porphyry and the deeper granodiorite layer, “biotite granite” GDC21-6000 (Hulen and Nielson, 1996) yielded a significantly younger U-Pb age of  $1.46 \pm 0.03$  Ma (MSWD = 2.1;  $n = 10$ ).

Granite sampled in well CA5636 23H 22-3242 may represent yet another intrusive phase. Although the samples represent a total depth range of  $\sim 735$  m, the orthopyroxene-biotite granite encountered throughout this interval was quite fresh and monotonously similar. Three samples (CA5636 74F 21-10500, -11700, and -12900) yielded ages indistinguishable within error ( $1.16 \pm 0.02$  Ma; MSWD = 0.1;  $N = 3$ ;  $n = 36$ ). The

comparative freshness of this material is consistent with it being one of the youngest intrusive rocks within the GPC.

#### 4.2.3. Dike crystallization ages

U-Pb zircon model ages for three dike samples from the southeastern GPC closely overlap with those from samples of the main body. Sample PDC2-6720 yielded an age ( $1.67 \pm 0.05$  Ma; MSWD = 8.4;  $n = 11$ ) similar to the age range of the microgranite porphyry, whereas the granitic dike sample CA5636 23H 22-3242 ( $1.30 \pm 0.03$  Ma; MSWD = 1.9;  $n = 7$ ) has an age similar to the orthopyroxene-biotite granite. The youngest U-Pb zircon age of all plutonic samples from the GPC was obtained from the quartz-poor alkalifeldspar

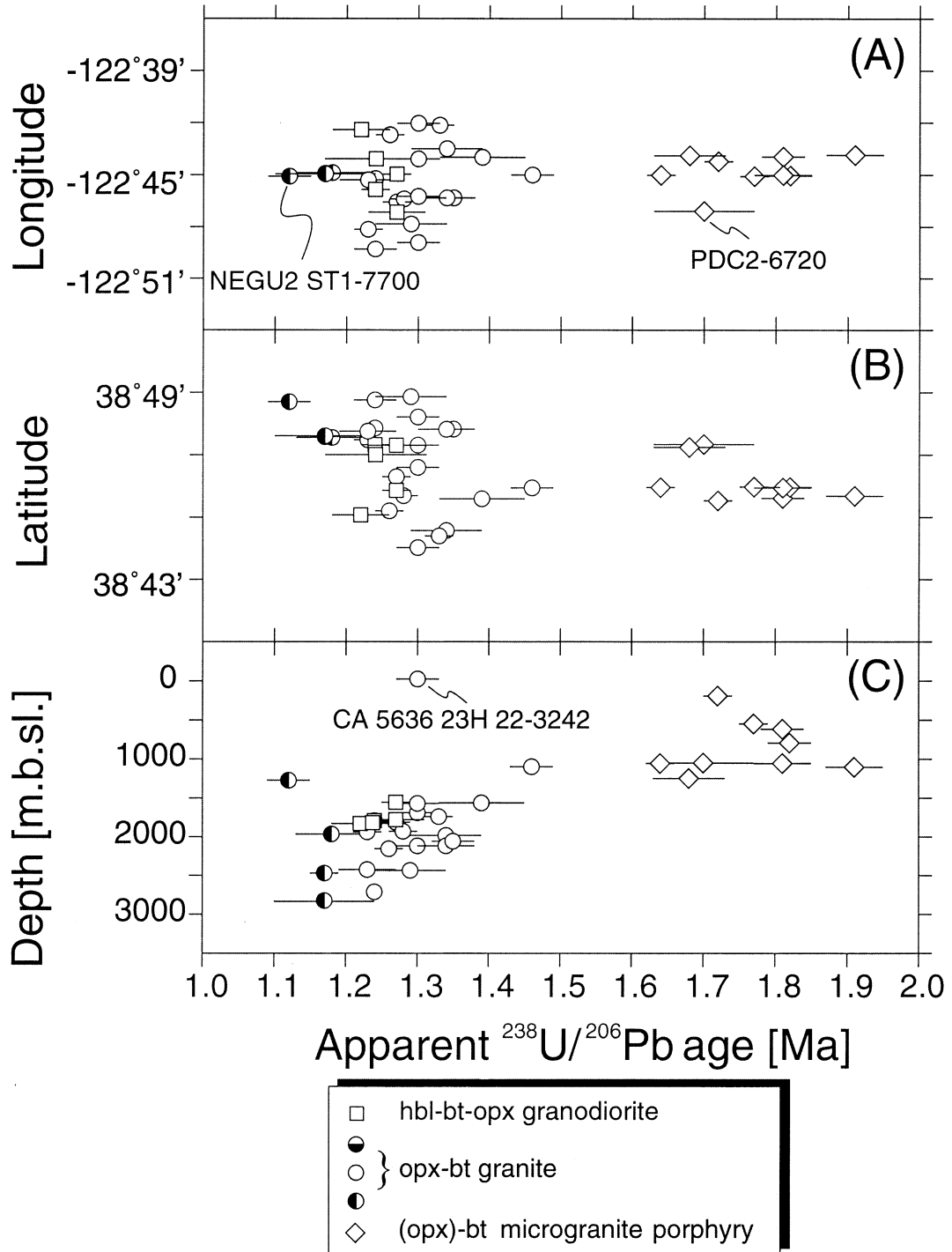


Fig. 6.  $^{207}\text{Pb}$ -corrected and disequilibrium corrected  $^{238}\text{U}/^{206}\text{Pb}$  model ages vs. a) longitude, b) latitude and c) depth.

granite dike (NEGU2 ST1-7700):  $1.11 \pm 0.03$  Ma (MSWD = 1.2; n = 5). This age overlaps within error with the younger orthopyroxene-biotite granite from well CA5636 74F 21.

The tonalite sample (PRATI25) is unique among our samples since it is a surface sample and the only felsic plutonic

rock that was known from the northwestern Geysers. In spite of a large amount of available material, only two zircon grains were recovered in the heavy mineral fraction. Both grains yielded Early Jurassic U-Pb ages (Fig. 4). Based upon these results and the intense low-temperature alteration exhibited by PRATI25 we conclude that the exposure is most likely an Early

Jurassic tectonic block present within the melange of the Franciscan subduction complex.

## 5. DISCUSSION

### 5.1. Heat Source of the Geysers Geothermal System

No active geothermal system on earth has been more extensively penetrated and explored than the steam field at the Geysers. The more than 700 deep wells that have been drilled over the past four decades have provided a remarkably complete transect of the field and the plutonic complex that underlies it. In spite of this, the nature and location of the upper crustal heat source remains unresolved. Petrologic investigations that harnessed the extensive sampling opportunities clearly indicate that the distribution of both the modern steam field and its liquid-dominated predecessor are spatially correlated to a high degree with the subsurface distribution of the GPC and its associated contact metamorphic aureole (Moore and Gunderson, 1995). While this apparent genetic relationship between these elements seems to indicate that the GPC is the shallow crustal heat source for the steam field, we have been unable to detect any intrusive rocks younger than 1 Ma in our detailed sampling of the GPC (Fig. 2).

The near coincidence our zircon U-Pb age results with previously determined terminal ages obtained in K-feldspar  $^{40}\text{Ar}/^{39}\text{Ar}$  step-heating experiments require that the zircon U-Pb ages closely date emplacement and crystallization of intrusive units of the GPC (i.e., to within  $\pm 0.1$  Ma; see Fig. 7). Accordingly, we conclude that the known extent of the GPC was emplaced between  $\sim 1.8$  and  $\sim 1.1$  Ma in at least three discrete pulses and that about 95% of the complex was emplaced between 1.2–1.4 Ma.

Faced with the constraints imposed by numerical heat flow simulations for the Geysers (Dalrymple et al., 1999; Norton and Hulen, 2001; Stimac et al., 2001), we are led to concur with Schriener and Suemnicht (1981) and others that the heat source of the steam field must fundamentally be related to a separate underlying pluton that probably was intruded much more recently ( $< 0.1$  Ma). Existence of such a body is supported by the following observations: 1) present-day heat flow in the area directly overlying the GPC is about three times higher than the average heat flow in the Clear Lake area (Walters and Combs, 1992; Fig. 1), although variability in the hydrologic properties of Franciscan and Clear Lake volcanic rocks might locally affect surface heat-flow; 2) temperature gradient studies in the northwest Geysers reveal evidence for significant cooling over the past 5000–10000 yr (Williams et al., 1993); and 3) a magmatic  $^3\text{He}$  signature is associated with the high-temperature reservoir from the northwest Geysers (Kennedy and Truesdell, 1996).

While our measurements do not offer a solution to the debate over the timing of intrusive activity beneath the northwest Geysers, they do provide some needed perspective. Specifically, the results demonstrate that the deep magma source region possessed a long-term viability underneath the GPC (between  $\sim 1.8$  and  $\sim 1.1$  Ma). In spite of this evidence for a long-lived source system, discrete age populations and the preservation of sharp compositional and textural contrasts within the GPC (e.g., GDC21-5865 leucocratic dike, or grano-

diorite in contact with coeval granite) rule out the existence of a persisting convecting magma chamber at the level of the GPC. The direct comparison of U-Pb zircon ages with results from K-Ar thermochronology firmly indicates rapid cooling and crystallization after emplacement at upper crustal levels.

Previous studies have shown that the locus of Coast Range volcanism progressively migrated northward (summarized in Donnelly-Nolan et al., 1993). With regard to felsic volcanism spatially associated with the Geysers steam field, the youngest eruption (Tyler Valley) occurred  $\sim 5$  km northwest of the steam reservoir at  $0.67 \pm 0.01$  Ma (Schmitt et al., this issue). The Tyler Valley eruption age also overlaps with the age of extensive hydrothermal alteration of the microgranite porphyry (Fig. 7) and  $^{40}\text{Ar}/^{39}\text{Ar}$  adularia ages from hydrothermal veins in the reservoir. Given this, it is clear that continued intrusion at this locale is in line with the previous magmatic history.

### 5.2. Relationship of the GPC to the Cobb Mountain Volcanic Center

In our companion paper (Schmitt et al., this issue) we discussed geochronologic and geochemical evidence that led us to conclude that zircon from the Cobb Mountain volcanic center crystallized from an initially undersaturated melt in a shallow crustal setting. Because the volcanic rocks that overlie the GPC are compositionally very similar to it (Fig. 3), and contain a zircon population that is indistinguishable from the main phase GPC (Fig. 4), it seems plausible that they were erupted from a molten portion of the GPC. We envision that these magma reservoirs were comparatively small and short-lived because K-feldspar  $^{40}\text{Ar}/^{39}\text{Ar}$  thermal history results indicate that the GPC cooled rapidly to below  $350^\circ\text{C}$  between 1.2–1.0 Ma (Dalrymple et al., 1999), the same interval over which Cobb Mountain was active (Schmitt et al., this issue). Hence it is clear that localized transient heating must have been involved if the Cobb Mountain volcanics were derived from the GPC. In Schmitt et al. (this issue), we postulated that episodic injections of mafic magmas in the Cobb Mountain area remelted portions of the GPC and that these transient magma bodies were erupted to form the Cobb Mountain volcanic center.

### 5.3. Significance of Previous Geochronology from the GPC

The spread in K-Ar (and  $^{40}\text{Ar}/^{39}\text{Ar}$ ) ages obtained from the GPC exceeds 2 Ma (0.57–2.7 Ma; see Table 1). It seems likely to us that loss of radiogenic  $^{40}\text{Ar}$  due to diffusion and recrystallization and/or incorporation of excess  $^{40}\text{Ar}$  largely account for this scatter. For example, in two instances,  $^{40}\text{Ar}/^{39}\text{Ar}$  ages predate U-Pb ages obtained from coexisting zircon by more than 1.0 Ma (Fig. 7). We believe that these younger  $^{40}\text{Ar}/^{39}\text{Ar}$  ages reflect recrystallization that was triggered by extensive hydrothermal alteration at high levels within the hydrothermal system. For example, K-feldspar from PDC2 yielded a  $^{40}\text{Ar}/^{39}\text{Ar}$  age of  $0.57 \pm 0.09$  Ma (Table 1; Pulka, 1991). This relatively young result is significant in that it has been previously reported as possible evidence for youthful intrusion beneath the southeast Geysers (see p. 1722 in Moore et al., 2000). Zircon results from this same dike sample indicate that this is not the case (Fig. 7). The much older U-Pb zircon age we

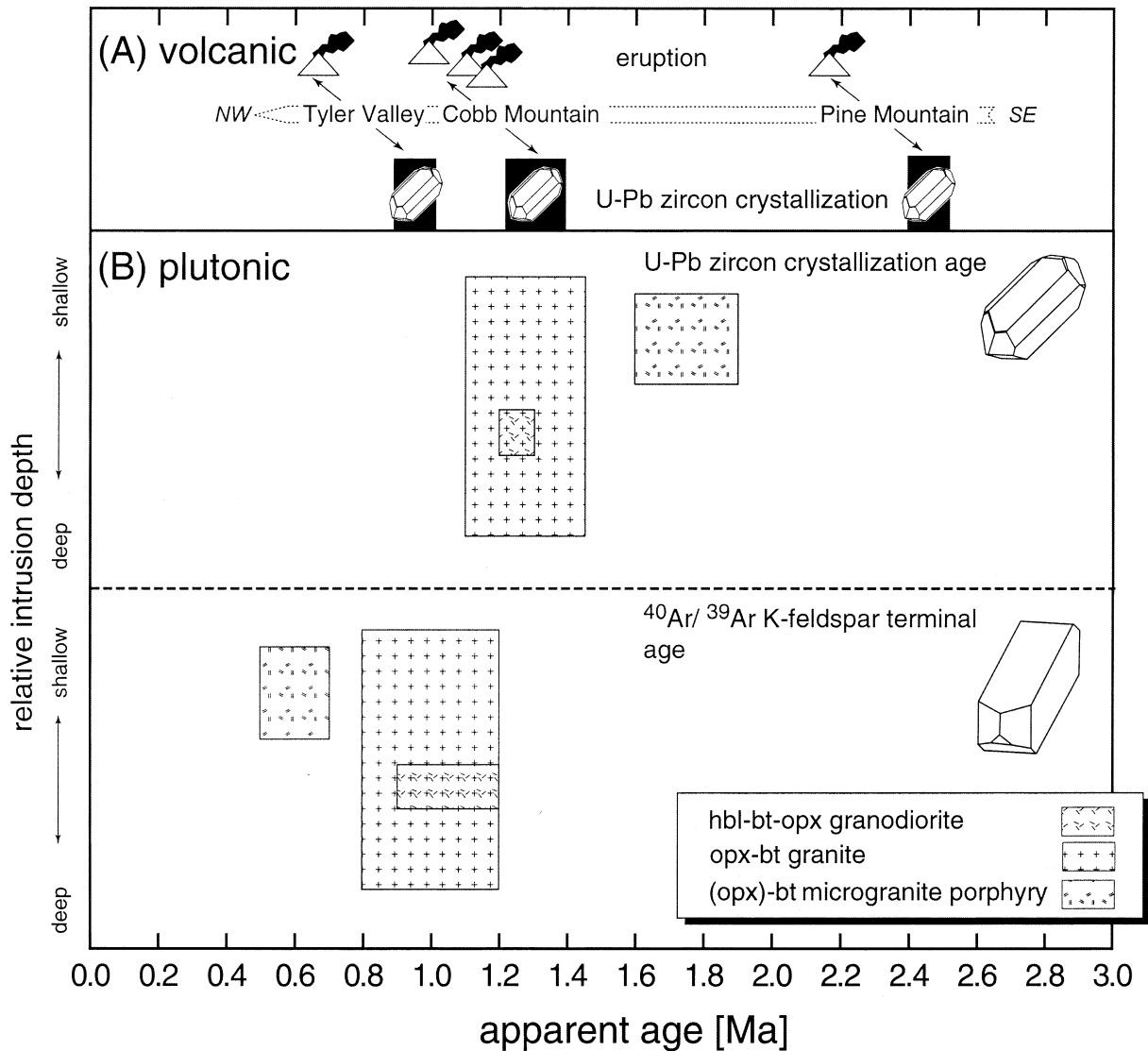


Fig. 7. Schematic magmatic history of the Geysers - Cobb Mountain magma system based on disequilibrium corrected  $^{238}\text{U}/^{206}\text{Pb}$  zircon model ages for GPC samples (lower panel; this study and Dalrymple et al., 1999) and associated felsic volcanic rocks (upper panel). We also indicate the range of  $^{40}\text{Ar}/^{39}\text{Ar}$  terminal K-feldspar step-heating ages for samples also analyzed for U-Pb zircon dating. Note strong discrepancy between terminal K-feldspar stepwise heating ages and zircon crystallization ages in particular for the hydrothermally altered shallow microgranite porphyry. Eruption ages for volcanic centers are based on sanidine  $^{40}\text{Ar}/^{39}\text{Ar}$  total fusion (Schmitt et al., this issue).

obtained ( $\sim 1.7 \pm 0.1$  Ma) is similar to results yielded by samples from the microgranite porphyry (Table 2). Moreover the petrologic and compositional characteristics of the PDC2 dike and the microgranite porphyry are identical (Fig. 3) and leave little doubt that the two are related. Microgranite porphyry sampled in DV2 also yields a  $^{40}\text{Ar}/^{39}\text{Ar}$  age that is much lower than the associated zircon age (Table 1 and 2; see also Fig. 7). In both instances (PDC2 and DV2) samples are noticeably altered.

There are other examples in which problematic Ar isotopic data may have led to erroneous conclusions regarding the longevity of hydrothermal systems. For example, Del Moro et al. (1982) and Villa and Puxeddu (1994) have interpreted biotite and K-feldspar  $^{40}\text{Ar}/^{39}\text{Ar}$  ages from the Larderello geo-

thermal field as indicating that the still-active geothermal system had persisted for up to 4 Ma at temperatures in excess of  $\sim 300^\circ\text{C}$ . We instead interpret the scatter of biotite ages and the poorly correlated  $^{40}\text{Ar}/^{39}\text{Ar}$  age and  $^{39}\text{Ar}$  diffusion spectra of K-feldspar (cf., Lovera et al., 2002) as likely effects of excess radiogenic argon ( $^{40}\text{Ar}_E$ ). Existence of  $^{40}\text{Ar}_E$  in the Larderello biotites is supported by the Del Moro et al. (1982) study of basement rocks in the Larderello field in which they found that biotite K-Ar ages tended to be higher than Rb/Sr ages determined from the same material. Regardless of these effects, our experience from the Geysers geothermal field leads us to conclude that K-Ar data do not provide a clear picture of the age of plutonic bodies associated with active geothermal fields.

#### 5.4. U-Pb Zircon Dating of the Geysers Plutonic Complex – Constraints for Pluton Emplacement

Rates and mechanisms of pluton emplacement remain a largely unresolved problem in the earth sciences in spite of more than 100 years of research (see Petford et al., 2000 for a review). Our results from the GPC demonstrate that considerable volumes of granitic magma ( $>300 \text{ km}^3$ ) can be emplaced and crystallize within the upper crust over a brief interval ( $\sim 0.2$  Ma). From the lateral dimensions of the main-phase plutonic body ( $\sim 3$  km) we estimate that space for the incoming magma was provided at a rate of  $\sim 15$  mm/yr.

Little is known about the tectonic environment that permitted this to occur, however. For example, while magmatic fluxes of the required magnitude can be easily attained if magma is delivered via dike conduits (Petford et al., 2000), space for the incoming magma must be made available at a sufficient rate. Host-rock displacement by extensional faulting is a particular favorable mechanism to provide this space (e.g., Hanson and Glazner, 1995; Yoshinobu et al., 1998). However, the preservation and NW-SE orientation of compositionally distinct units within the GPC (in particular the elongated body of granodiorite) is opposite to the predicted orientation of sheeting if the magma was emplaced in an extensional bend separating an échelon strike-slip faults (see Yoshinobu et al., 1998).

Alternatively, it is possible that emplacement of the GPC is related to a NE-SW zone of extension within the Geysers - Clear Lake region. Stanley et al. (1998) summarized evidence for such a zone of extension: (1) NE-trending faults within the Geysers define a pattern distinct from the regional fracture pattern (Fig. 1), (2) the youngest mafic volcanic vents in the Clear-Lake region are aligned SW-NE and (3) contours of elevated heat-flow extend from the Geysers to the NE (see Fig. 1; Hulen and Nielson, 1996). In spite of this, there is no independent evidence for extension of the magnitude and rate that is required by the age and dimensions of the GPC. In conclusion, while we as yet do not understand details of the emplacement process of the GPC, our newly obtained results place tighter constraints upon pluton formation rates than have been generally possible.

#### 6. SUMMARY AND CONCLUSIONS

- (1) We interpret the paucity of relict zircon in GPC samples and low Zr contents in quartz-hosted melt inclusions from compositionally equivalent volcanic rocks (Schmitt et al., this issue) as evidence that the GPC magmas were initially undersaturated in zircon (Watson and Harrison, 1983). Hence, zircon U-Pb ages likely record the time when the host magma cooled below temperatures required for zircon saturation after emplacement at shallow levels. Experimentally determined Pb diffusion rates indicate essentially complete closure at magmatic temperatures relevant to the GPC (Cherniak and Watson, 2000) and imply that U-Pb parent-daughter relations remained undisturbed under conditions prevailing during the postcrystallization history of the GPC.
- (2) Our U-Pb zircon ages thus allow us to reconstruct the crystallization history of the GPC that spans between  $\sim 1.8$  and  $\sim 1.1$  Ma. In some instances (wells PDC and DV2), U-Pb zircon ages are by about 1 Ma older than previous

age interpretations based on K-feldspar Ar isotopic measurements. From our experience in the Geysers, we therefore urge caution in the use of Ar isotope analyses to determine pluton intrusion ages in active geothermal systems.

- (3) The U-Pb zircon ages from the GPC strongly correlate with its internal petrologic structure known from geothermal well penetration: compositional heterogeneities and sharp age gradients are well preserved and rule out the possibility that, at its known extent, the GPC ever existed as a single convecting magma system. Furthermore, overlapping zircon crystallization and K-feldspar cooling ages indicate rapid ( $\sim 0.2$ – $0.4$  Ma) cooling to temperatures  $<350^\circ \text{C}$  (Dalrymple et al., 1999).
- (4) Indistinguishable U-Pb ages in main-phase GPC and Cobb Mountain volcanic rocks that erupted  $\sim 0.2$ – $0.3$  Ma after zircon crystallization are best explained by zircon recycling caused by episodic remelting of portions of the GPC. The zircon U-Pb age relationships between main-phase GPC and volcanic samples indicate that the locus of magmatism remained centered beneath the Geysers reservoir for nearly a million years and that thermal rejuvenation episodically occurred. This perception is underlined by results of numerical heat flow simulations for the Geysers (Dalrymple et al., 1999; Stimac et al., 2001; Norton and Hulen et al., 2001) that indicate that in addition to the intrusive mass of the GPC, other – yet undiscovered – heat sources are required to sustain the geothermal system up to present day.
- (5) With regard to the thermal evolution of the Geysers steam field, we envisage the following scenario: (a) a large deeper-rooted source region persisted beneath the Geysers since  $\sim 2$  Ma; (b) dominantly rhyolitic magmas episodically ascended from this source region and intruded into shallow crustal levels forming the composite GPC. (c) Periodic injection of mafic magma reactivated portions of the GPC causing eruption of rhyolitic and mixed intermediate magmas from the overlying Cobb Mountain center. The overall thermal effect of continued episodic magma injections sustained a long-lived upper-crustal magmatic-hydrothermal system consistent with thermal history models presented in Dalrymple et al. (1999).

*Acknowledgments*—This research was conducted under the auspices of Department of Energy grant DE-FG-03-89ER14049 and the instrumentation and facilities grant NSF grant EAR-0113563 to Harrison, McKeegan, and Reid. We thank Tom Box, Mitch Stark, and Joe Beall at Calpine for discussions, their support in securing samples from the Cobb Mountain area, and information regarding sample coordinates. Bill Smith (NCPA) is thanked for access to samples from the southernmost Geysers. Dave Langton (EGI) assisted us in retrieving samples from the EGI geothermal sample laboratory. Ainslie Harrison aided in mineral separation. Chris Coath (U-Pb) was instrumental in obtaining the isotopic age results. We thank Rudi Naumann and Jörg Erzinger of the GeoForschungsZentrum Potsdam for their generous support in obtaining XRD modal analysis results from borehole samples. Comments by Julie Donnelly-Nolan and journal reviewers are gratefully acknowledged. Yuri Amelin is thanked for editorial handling.

*Associate editor:* Y. Amelin

## REFERENCES

- Baldwin S. L. and Ireland T. R. (1995) A tale of two eras: Pliocene-Pleistocene unroofing of Cenozoic and late Archean zircons from active metamorphic core complexes, Solomon Sea, Papua New Guinea. *Geology* **23**, 1023–1026.
- Barker B. J., Gulati M. S., Bryan M. A., and Riedel K. L. (1992) Geysers reservoir performance. In *Monograph on The Geysers Geothermal Field* (ed. C. Stone), Geothermal Research Council Special Report **17**, Davis, California, pp. 167–177.
- Blackwell D. D. and Steele J. L. (1992) *DNAG Geothermal Map of North America*. (1:5,000,000). Geol. Soc. Am., Boulder, Colorado.
- Cherniak D. J. and Watson E. B. (2000) Pb diffusion in zircon. *Chem. Geol.* **172**, 5–24.
- Dalrymple G. B. (1993) Preliminary report on  $^{40}\text{Ar}/^{39}\text{Ar}$  incremental heating experiments on feldspar samples from the felsite unit, Geysers geothermal field, California. In *Active Geothermal Systems and Gold-Mercury Deposits in the Sonoma-Clear Lake Volcanic Fields, California* (ed. J. J. Rytuba), Society of Economic Geologists Guidebook Series **16**, Littleton, Colorado, pp. 131–140.
- Dalrymple G. B., Grove M., Lovera O. M., Harrison T. M., Hulen J. B., and Lanphere M. A. (1999) Age and thermal history of The Geysers plutonic complex (felsite unit), Geysers geothermal field, California; a  $^{40}\text{Ar}/^{39}\text{Ar}$  and U-Pb study. *Earth Planet. Sci. Lett.* **30**, 285–298.
- DeGraaff-Surpless K., Graham S. A., Wooden J. L., and McWilliams M. O. (2002) Detrital zircon provenance analysis of the Great Valley Group, California: Evolution of an arc-forearc system. *Geol. Soc. Am. Bull.* **114**, 1564–1580.
- Del Moro A., Puxeddu M., Radicati di Brozolo F., and Villa I. M. (1982) Rb-Sr and K-Ar ages on minerals at temperatures of 300° – 400° C from deep wells in the Larderello geothermal field (Italy). *Contrib. Mineral. Petrol.* **81**, 340–349.
- Dickinson W. R. and Snyder W. S. (1979) Geometry of triple junctions related to San Andreas transform. *J. Geophys. Res.* **84**, 561–572.
- Doi N., Kato O., Ikeuchi K., Komatsu R., Miyazaki S.-I., Akaku K., and Uchida T. (1998) Genesis of the plutonic-hydrothermal system around Quaternary granite in the Kakkonda geothermal system, Japan. *Geothermics* **27**, 663–690.
- Donnelly-Nolan J. M., Hearn Jr. B. C., Curtis G. H., and Crake R. E. (1981) Geochronology and evolution of the Clear Lake volcanics. *U. S. Geol. Survey Prof. Pap.* **1141**, 47–60.
- Donnelly-Nolan J. M., Burns M. G., Goff F. E., Peters E. K., and Thompson J. M. (1993) The Geysers-Clear Lake area, California: Thermal waters, mineralization, volcanism, and geothermal potential. *Econ. Geol.* **88**, 301–316.
- Emmermann R. and Lauterjung J. (1990) Double X-ray analysis of cuttings and rock flour; a powerful tool for rapid and reliable determination of borehole lithostratigraphy. *Scientific Drilling* **1**, 269–282.
- Getty S. R. and DePaolo D. J. (1995) Quaternary geochronology using the U-Th-Pb method. *Geochim. Cosmochim. Acta* **59**, 3267–3272.
- Hanson R. F. and Glazner A. F. (1995) Thermal requirements for extensional emplacement of granitoids. *Geology* **23**, 213–216.
- Hochstein M. P. (1995) Crustal heat transfer in the Taupo volcanic zone (New Zealand): Comparison with other volcanic arcs and explanatory heat source models. *J. Volcanol. Geothermal Res.* **68**, 117–151.
- Hearn B. C., Donnelly-Nolan J. M., and Goff F. E. (1995) Geologic map and structure sections of the Clear Lake volcanics, Northern California. Scale 1:24,000. *U.S. Geol. Survey Map* **I-2362**.
- Hulen J. B. and Nielson D. L. (1993) Interim report on geology of The Geysers felsite, Northwestern California. *Geothermal Resources Council Trans.* **17**, 249–258.
- Hulen J. B. and Walters M. A. (1993) The Geysers felsite and associated geothermal systems, alteration, mineralization and hydrocarbon occurrences. In *Active Geothermal Systems and Gold-Mercury Deposits in the Sonoma-Clear Lake Volcanic Fields, California* (ed. J. J. Rytuba), Society of Economic Geologists Guidebook Series **16**, Littleton, Colorado, pp. 141–152.
- Hulen J. B. and Nielson D. L. (1996) The Geysers felsite. *Geothermal Resources Council Trans.* **20**, 295–306.
- Hulen J. B., Heizler M. T., Stimac J. A., Moore J. N., and Quick J. C. (1997) New constraints on the timing of magmatism, volcanism, and the onset of vapor-dominated conditions at The Geysers steam field, California. *Proceedings of the Twenty-Second Workshop on Geothermal Reservoir Engineering*, Stanford University, Stanford, California, pp. 75–81.
- Johnson C. M. and O'Neil J. R. (1984) Triple junction magmatism: A geochemical study of Neogene volcanic rocks in western California. *Earth Planet. Sci. Lett.* **71**, 242–262.
- Kennedy B. M. and Truesdell A. H. (1996) The Northwest Geysers high-temperature reservoir: Evidence for magmatic degassing and implications for the origin of The Geysers geothermal field. *Geothermics* **25**, 365–387.
- Le Bas M. J. and Streckeisen A. L. (1991) The IUGS systematics of igneous rocks. *J. Geol. Soc. London* **148**, 825–833.
- Lovera O. M., Grove M., and Harrison T. M. (2002) Systematic analysis of K-feldspar  $^{40}\text{Ar}/^{39}\text{Ar}$  step heating results II: Relevance of laboratory argon diffusion properties to nature. *Geochim. Cosmochim. Acta* **66**, 1237–1255.
- Lowenstern J. B., Janik C. J., Fahlquist L. S., and Johnson L. S. (1999) Gas and isotope geochemistry of 81 steam samples from wells in The Geysers Geothermal field, Sonoma and Lake counties, California, USA. *U. S. Geol. Survey Open-file Rep.* **99-304**, 1–23.
- Mahon K. I. (1996) The new “York” regression; application of an improved statistical method to geochemistry. *Intern. Geol. Rev.* **38**, 293–303.
- Mankinen E. A., Donnelly J. M., and Grommé C. S. (1978) Geomagnetic polarity event recorded at 1.1 m.y. B.P. on Cobb Mountain, Clear Lake volcanic field, California. *Geology* **6**, 653–656.
- McLaughlin R. J., Moore D. E., Sorg D. H., and McKee E. H. (1983) Multiple episodes of hydrothermal circulation thermal metamorphism, and magma injection beneath the Geysers steam field, California. *Geological Society of America Abstracts with Programs* **15**, 417 (abstr.).
- Moore J. N. and Gunderson R. P. (1995) Fluid inclusion and isotopic systematics of an evolving magmatic-hydrothermal system. *Geochim. Cosmochim. Acta* **59**, 3887–3907.
- Moore J. N., Adams M. C., and Anderson A. J. (2000) The fluid inclusion and mineralogical record of the transition from liquid- to vapor-dominated conditions in the Geysers geothermal system, California. *Econ. Geol.* **95**, 1719–1737.
- Moore J. N., Norman D. I., and Kennedy B. M. (2001) Fluid inclusion gas compositions from an active magmatic-hydrothermal system: A case study of the Geysers geothermal field. *Chem. Geol.* **173**, 3–30.
- Norton D. L. and Hulen J. B. (2001) Preliminary numerical analysis of the magma-hydrothermal history of The Geysers geothermal system, California, USA. *Geothermics* **30**, 211–234.
- Petford N., Cruden A. R., McCaffrey K. J. W., and Vigneresse J.-L. (2000) Granite magma formation, transport and emplacement in the Earth's crust. *Nature* **408**, 689–673.
- Pulka F. S. (1991) Subsurface geology at Ford Flat, Geysers geothermal field, northern California. M. Sc. Thesis, Michigan Tech. Univ.
- Sañudo-Wilhelmy S. A. and Flegal A. R. (1994) Temporal variations in lead concentrations and isotopic composition in the Southern California Bight. *Geochim. Cosmochim. Acta* **58**, 3315–3320.
- Schmitt A. K., Grove M., Harrison T. M., Lovera O., Hulen J. B., and Walters M. (2002) The Geysers - Cobb Mountain Magma System, California. (Part 1): U-Pb zircon ages of volcanic rocks, conditions of zircon crystallization and magma residence times. *Geochim. Cosmochim. Acta* **67**, 3423–3442.
- Schriener A. Jr. and Suemnicht G. A. (1981) Subsurface intrusive rocks at The Geysers geothermal area, California. In *Proceedings of the Symposium on Mineral Deposits of the Pacific Northwest* (eds. M. L. Silberman, C. W. Field, and A. L. Berry), *U. S. Geol. Survey Open-file Rep.* **81-355**, 295–302.
- Shook G. M. (1995) Development of a vapor-dominated reservoir with a “high-temperature” component. *Geothermics* **24**, 489–505.
- Sorey M. L., Lewis R. E., and Olmsted F. H. (1978) The hydrothermal system of Long Valley Caldera, California. *U. S. Geol. Survey Prof. Pap.* **P 1044-A**, 1–60.
- Stanley W. D., Benz H. M., Walters M. A., Villseñor A., and Rodriguez B. D. (1998) Tectonic controls on magmatism in The Geysers-Clear Lake region: Evidence from new geophysical models. *Geol. Soc. Am. Bull.* **110**, 1193–1207.

- Stimac J. A., Goff F. A., and Wohletz K. (2001) Thermal modeling of the Clear Lake magmatic-hydrothermal system, California, USA. *Geothermics* **30**, 349–390.
- Tagami T. and Dumitru T. A. (1996) Provenance and thermal history of the Franciscan accretionary complex – Constraints from zircon fission track thermochronology. *J. Geophys. Res.* **B 101**, 11353–11364.
- Thompson R. C. (1992) Structural stratigraphy and intrusive rocks at The Geysers geothermal field. In *Monograph on The Geysers Geothermal Field* (ed. C. Stone), Geothermal Research Council Special Report **17**, Davis, California, pp. 59–63.
- Thompson R. C. and Gunderson R. P. (1992) The orientation of steam-bearing fractures at The Geysers geothermal fields. In *Monograph on The Geysers Geothermal Field* (ed. C. Stone), Geothermal Research Council Special Report **17**, Davis, California pp. 65–68.
- Turrin B.D., Donnelly-Nolan J.M., and Hearn B.C. Jr. (1994)  $^{40}\text{Ar}/^{39}\text{Ar}$  ages from the rhyolite of Alder Creek, California: Age of the Cobb Mountain normal-polarity subchron revisited. *Geology* **22**, 251–254.
- Unocal Corporation, Geysers Geothermal Company, NCPA, GEO Operator Corporation, Santa Fe Geothermal and California Department of Water Resources. (1992) Geysers top-of-felsite-map. In *Monograph on The Geysers Geothermal Field* (ed. C. Stone), Geothermal Research Council Special Report **17**, Davis.
- Villa I. M. and Puxeddu M. (1994) Geochronology of the Larderello geothermal field; new data and the “closure temperature” issue. *Contrib. Mineral. Petrol.* **115**, 415–426.
- Walters M. A. and Combs J. (1992) Heat flow in The Geysers-Clear Lake Geothermal area of northern California, USA. In *Monograph on The Geysers Geothermal Field* (ed. C. Stone), Geothermal Research Council Special Report **17**, Davis, California, pp. 43–53.
- Walters M. A., Sternfeld J. N., Haizlip J. R., Drenick A. F., and Combs J. (1992) A vapor-dominated high-temperature reservoir at The Geysers, California. In *Monograph on The Geysers Geothermal Field* (ed. C. Stone), Geothermal Research Council Special Report **17**, Davis, pp. 77–87.
- Watson E. B. and Harrison T. M. (1983) Zircon saturation revisited; temperature and composition effects in a variety of crustal magma types. *Earth Planet. Sci. Lett.* **64**, 295–304.
- White D. E., Hutchinson R. A., and Keith T. E. C. (1989) The geology and remarkable thermal activity of Norris Geyser Basin, Yellowstone National Park, Wyoming. *U. S. Geol. Survey Prof. Pap.* **1456**, 1–84.
- Wiedenbeck M., Alle P., Corfu F., Griffin W. L., Meier M., Oberli F., Von Quadt A., Roddick J. C., and Spiegel W. (1995) Three natural zircon standards for U-Th-Pb, Lu-Hf, trace element and REE analyses. *Geostandards Newslett.* **91**, 1–23.
- Williams C.F., Galanis S.P. Jr., Moses T.H. Jr., and Grubb F.V. (1993) Heat-flow studies in the Northwest Geysers geothermal field, California. *Geothermal Research Council Transactions* **17**, 281–288.
- WoldeGabriel G., Goff F., and Aronson J. (2001) Mineralogy and K-Ar geochronology of mixed-layered illite/smectite from The Geysers coring project, California, USA. *Geothermics* **30**, 193–210.
- Yoshinobu A. S., Okaya D. A., and Paterson S. R. (1998) Modeling the thermal evolution of fault-controlled magma emplacement models: Implications for the solidification of granitoid plutons. *J. Structural Geol.* **20**, 1205–1218.